# RSC Advances

Accepted Manuscript

This article can be cited before page numbers have been issued, to do this please use: C. Han, L. Yang, P. Raghunath, M. C. Lin, R. Kumar and H. Lin, *RSC Adv.*, 2016, DOI: 10.1039/C6RA19266A.

View Article Online
DOI: 10.1039/C6RA19266A

RSC Advances

RSCPublishing

ARTICLE



Cite this: DOI: 10.1039/x0xx00000x

# Lateral fluoro-substitution and chiral effects on supramolecular liquid crystals containing rod-like and H-bonded bent-core mesogens

Chun-Chieh Han,[a] Li-Han Yang,[a] Putikam Raghunath,[b] Ming-Chang Lin[b], Rohit Kumar[a] and Hong-Cheu Lin*[a]

Received ooth January 2012,
Accepted ooth January 2012

DOI: 10.1039/x0xx00000x

www.rsc.org/

The first series of liquid crystalline supramolecular diads **C**/**D** containing asymmetric rod-like and H-bonded bent-core mesogens were designed and synthesised, among which supramolecular diad $\mathbf{P_{III}}$*/$\mathbf{A_{II}}$* with two chiral centers on both H-acceptor/H-donor and non-lateral fluoride substitution possessed a wide blue phase (BPI) range of 13.7°C. According to the molecular modeling, a large biaxial parameter (≥3.2) and an appropriate HTP value (4.2~4.8 $\mu m^{-1}$) are the most important factors to stabilize the double twisted cylinder structure (i.e., BPI) in supramolecular diads. Moreover, the bent angles, biaxial parameters and dipole moments of supramolecular diads are mainly affected by the locations and numbers of H-bonds and chiral centers. Not only larger bent angles and biaxial parameters but also smaller dipole moments and HTP values were obtained by removing the lateral fluoride substitution on supramolecular diads to achieve the blue phase of $\mathbf{P_{III}}$*/$\mathbf{A_{II}}$* (without lateral fluoride substitution). Finally, the special optimal 1:1 molar ratio of supramolecular diad $\mathbf{P_{III}}$*/$\mathbf{A_{II}}$* (i.e., H-donor=50 mol%) with the widest blue phase range is mainly attributed to its rod-like and H-bonded bent-core mesogens, rather than H-donor=75 mol% in most supramolecular complexes containing linear H-bonded rod-like mesogens.

## Introduction

The blue phases (BPs), i.e., PPI, BPII and BPIII, are liquid crystalline (LC) phases between isotropic and cholesteric phases upon heating or cooling within narrow ranges. The molecular structures of BPs were considered double twisted cylinders (DTCs),[1,2] and the DTCs were often introduced by mixing either biaxial components to the cholesteric phase having high chiralities[3,4] or chiral dopants to the nematic phase possessing high biaxialities.[5,6] According to Kossel diagrams,[7,8] Landau theory[9,10] and polarizing optical microscopy of previous researches, the PPI, BPII and BPIII can be categorized into three types of packing arrangements as body-center cubic, simple cubic[11-13] and isotropic (with an arbitrary orientation)[14] structures, respectively. The BPs are used for new applications exhibiting no birefringence but selective reflection of circularly polarized light,[15,16] including fast light modulators,[17] large-screen flat panel displays,[18] three-dimensional BP lasers,[19-21] and tunable photonic band gap materials.[22-24] However, the narrow temperature ranges (usually about 1°C) of BPs devastated the possible applications of BPLC materials.[25] So far, various methods were applied to introduce BPs or extend the temperature ranges of BPs, such as: supercooled freezing stabilization,[26] polymer stabilization,[27-30] nanoparticle stabilization,[31,32] light induction,[33,34] bent-core LCs,[35-39] hydrogen-bonded LCs[40-42] and discotic LCs.[43] However, most BPLC materials with wide BP ranges were obtained from LC mixtures by above methods. The BP mixtures increased the complexities of the ingredients, so the factors to influence the BPs could not be analyzed easily. Therefore, the developments of single-component BPLC materials with both biaxialities and chiralities are more important to understand the formation and optimization of BPs.[44-46]

In the previous literature, both chiralities and biaxialities are important factors to be responsible for the appearance of BPs in single-component and mixture materials. For instance, the influences of achiral bent-core molecules where like some

[a]*Department of Materials Science and Engineering, National Chiao Tung University, Hsinchu, Taiwan. Fax: (+886)35724727*
*E-mail: linhc@mail.nctu.edu.tw*

[b]*Department of Applied Chemistry, National Chiao Tung University, Hsinchu, Taiwan. Fax: (+886)35712179*

Footnotes relating to the title and/or authors should appear here. Electronic Supplementary Information (ESI) available: [details of any supplementary information available should be included here]. See DOI: 10.1039/x0xx00000x

View Article Online
DOI: 10.1039/C6RA19268A
Journal Name



nanostructuring with chirality[47-49] on enhancing chirality of LCs were also reported.[50,51] Moreover, the temperature ranges of BPs could be broadened by doping bent-core molecules with large biaxialities in cholesteric hosts,[52,53] or by doping molecules with strong chiralities in biaxial LC nematic hosts (e.g., bent-core or di-mesogenic structures).[54,55] In addition, asymmetric di-mesogenic molecules[44-46,56] (including T-shape)[45,46,56] and symmetric dimeric molecules[57-62] (including U-shape)[63,64] containing odd-number linking groups were also used to stabilize the DTC structures and extend the temperature ranges of BPs. Thus, the asymmetric di-mesogenic molecule containing the bent-core structure is one of the widely used structures to stabilize BPs and extend BP ranges.[44]

In biological systems, hydrogen bonds play important roles for the assembly of supramolecules, due to strong intermolecular interactions. The hydrogen-bonded (H-bonded) structures were not only to construct supramolecular structures but also to generate functional soft materials.[65,66] Moreover, the intermolecular hydrogen bonding of two complimentary molecules can be formed by hydrogen-bonded (H-bonded) donors (e.g., benzoic acids) and acceptors (e.g., pyridyl derivatives).[67-69] Therefore, in H-bonded LCs (e.g., LCs diads or complexes), the compositions can be formed by self-assembly of supramolecular force, and the diversified molecular structures can be prepared by hydrogen-bonded, simply. In previous researches, the flexible hydrogen bonds can not only facilitate better mesomorphic properties of LC materials but also stabilize BPLCs effectively.[70,71] Therefore, we have a great interest to introduce supramolecular structures to asymmetric di-mesogenic LC molecules possessing covalent rod-like and H-bonded bent-core mesogens.

In our study, we design and synthesize a series of supramolecular liquid crystals containing rod-like and H-bonded bent-core mesogens, where the diads were self-assemblied by the same molar number of H-acceptors **C** and H-donors **D**. where H-acceptors **C** were $\mathbf{P_{III}}$, $\mathbf{P_{III}}$* and $\mathbf{P_{II}}$*, and H-donors **D** were $\mathbf{A_{II}}$, $\mathbf{A_{II}}$*, $\mathbf{A_{II}F}$, $\mathbf{A_{II}F}$* and $\mathbf{A_{III}F}$*. All physical properties (including phase transition temperatures) of supramolecular liquid crystals containing rod-like and H-bonded bent-core diads could be acquired by DSC and POM. The influences of H-bonded positions, numbers of chiral centers and lateral fluoro-substitutions to affect the formation and the ranges of BPs are also well developed and discussed in this report.

## Experimental

### Chemical and physical analysis

$^1$H NMR spectra were recorded on a Bruker Unity 300 MHz spectrometer using $CDCl_3$ as a solvent. Elemental analyses (EA) were performed on a Heraeus CHN-OS RAPID elemental analyzer. The FTIR spectra were recorded on a PerkinElmer spectrum 1000. The UV-visible spectra were recorded on a JASCO V-670 spectrometer with 2 nm resolution at the BP phase.

### Molecular simulation method

To gain insight into the electronic structures of various supramolecular diads **C/D** (where H-acceptors **C** = $\mathbf{P_{III}}$, $\mathbf{P_{III}}$* and $\mathbf{P_{II}}$*; H-donors **D** = $\mathbf{A_{II}}$, $\mathbf{A_{II}}$*, $\mathbf{A_{II}F}$, $\mathbf{A_{II}F}$* and $\mathbf{A_{III}F}$*) at a molar ratio of H-acceptors and H-donors = 1:1 (mol/mol), the studies of density functional theory (DFT) calculations were carried out by using the Gaussian09 software package.[72] Geometry optimizations of all ground state hydrogen-bonded structures were done by B97D Grimme's functional including dispersion corrections[73] using the standard 6-31G(d,p) basis set. It was found that the performance of B97D method is remarkably good and reaching average on the CCSD(T) accuracy for non-covalently bound systems, including many pure van der Waals complexes.[73] The obtained minima were further confirmed by vibrational frequency calculations at the same level; only the lowest energy conformation is reported here. The electrostatic surface potential (ESP) was calculated using the Merz-Singh-Kollman (MK) scheme[74] at the B97D/6-31G(d,p) level of theory.

### Liquid crystalline and physical properties

Mesophasic textures of various supramolecular diads were characterized through polarizing optical microscopy (POM) using a Leica DMLP equipped with a temperature control hot stage (Mettler Toledo FP82HT). Temperatures and enthalpies of phase transitions were determined by differential scanning calorimetry (DSC, model: Perkin Elmer Pyris 7) under $N_2$ at a heating and cooling rate of 0.5°C/min. The transition temperatures of BPI-cholesteric (N*) was determined by POM upon a cooling rate of 0.5°C/min, due to the undetectable enthalpy changes by DSC. Infrared (IR) spectra were obtained by a Perk-Elmer Spectrum 100 instrument. The FTIR spectra were recorded on a PerkinElmer spectrum 1000. The UV-visible spectra were recorded on a JASCO V-670 spectrometer with 2 nm resolution at room temperature. Synchrotron powder X-ray diffraction (XRD) measurements were performed at beamline 17A1 of the National Synchrotron Radiation Research Center (NSRRC), Taiwan; the wavelengths of the X-rays ranged from 1.0243 to 1.3302 Å. The powder samples were packed into capillary tubes or dropped on an untreated cover glass and then heated with a heat gun, whose temperature controller was programmable by a computer having a PID feedback system. The scattering angle (θ) was calibrated using a mixture of silver behenate and silicon. The helical twist power (HTP) measurements of all supramolecular diads **C/D** = 1:1 mol/mol were performed using a UV-vis spectrophotometer (Jasco V-670) and Cano wedge cells, where the commercial LC, i.e., JC1041-XX (Chisso), was used as a host material.

### Preparation of materials

The syntheses of H-acceptors ($\mathbf{P_{III}}$, $\mathbf{P_{III}}$* and $\mathbf{P_{II}}$*) and H-donors ($\mathbf{A_{II}}$, $\mathbf{A_{II}}$*, $\mathbf{A_{II}F}$, $\mathbf{A_{II}F}$* **and** $\mathbf{A_{III}F}$*) of supramolecular diads **C/D** (**C** = $\mathbf{P_{III}}$ and $\mathbf{P_{III}}$*; **D** = $\mathbf{A_{II}}$, $\mathbf{A_{II}}$*, $\mathbf{A_{II}F}$ and $\mathbf{A_{II}F}$*) and $\mathbf{P_{II}}$*/$\mathbf{A_{III}F}$* are shown in Scheme 1, where their synthetic details are also illustrated in the supporting information and Schemes S1 and S2.

View Article Online
DOI: 10.1039/C6RA19266A ARTICLE



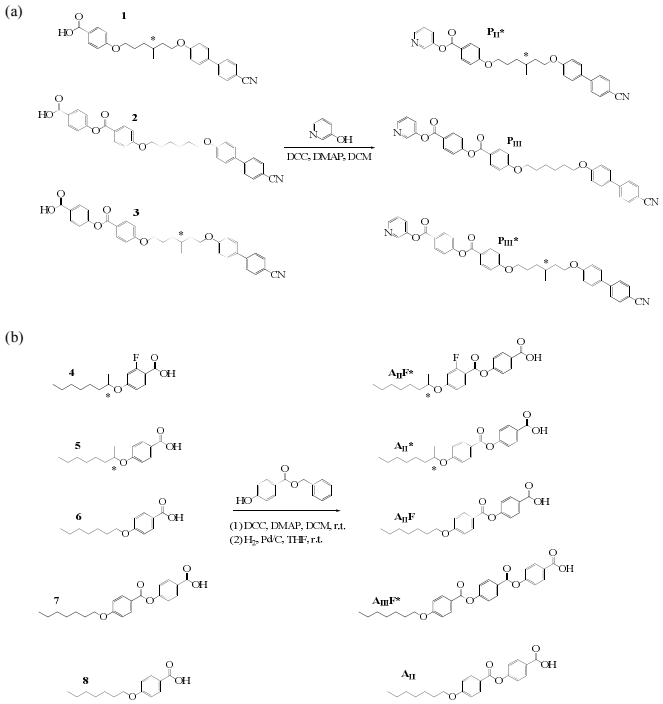


**Scheme 1** Synthesis of (a) H-acceptors ($\mathbf{P_{III}}$, $\mathbf{P_{III}}$* and $\mathbf{P_{II}}$*) and (b) H-donors ($\mathbf{A_{II}}$, $\mathbf{A_{II}}$*, $\mathbf{A_{II}F}$, $\mathbf{A_{II}F}$* and $\mathbf{A_{III}F}$*).

**(i) H-acceptor $\mathbf{P_{II}}$*.** Compound **1** (2 g, 3.81 mmol), pyridin-3-ol (0.34 g, 4.6 mmol) and DMAP (0.05 g, 0.381 mmol) were dissolved in dry DCM (100 ml) in nitrogen system, then DCC (2.38 g, 11.43 mmol) was added in the solution. The solution was reacted for 16 hours at room temperature. After reaction, the mixture filtrated and then washed with DCM. The solution was extracted with deionized water/DCM, then obtained the organic phase of solution. The organic phase was dried by $MgSO_4$ and concentrated using a rotary evaporator. The residue was purified by column chromatography on silica (*n*-hexane/DCM = 5:3, v/v). The final product as a white solid has a yield of 60%. $^1$H NMR (300 MHz, $CDCl_3$) δ(ppm): 8.6 (s, 1H, pyridine-H), 8.50 (d, $J$ = 6.8 Hz, 1H, pyridine-H), 8.05 (d, $J$ = 7.9 Hz, 2H, Ar-H), 7.88 (s, 4H, Ar-H), 7.75 (d, $J$ = 8.1 Hz, 2H, Ar-H), 7.70 (d, $J$ = 7.4 Hz, 1H, pyridine-H), 7.52 (d, $J$ = 7.2 Hz, 1H, pyridine-H), 7.15 (d, $J$ = 8.3 Hz, 2H, Ar-H), 7.05 (d, $J$ = 8.4 Hz, 2H, Ar-H), 4.12 (t, $J$ = 8.6 Hz, 4H, -$OCH_2$-), 1.90-1.71 (m, 5H, -$CH_2$-), 1.75-1.43 (m, 2H, -$CH_2$-), 1.01 (d, $J$ = 8.7 Hz, 3H, -$CH_3$). Anal. Calcd for $C_{32}H_{30}N_2O_4$: C 75.87, H 5.97, N 5.53; Found: C 75.49, H 5.91, N 5.49. MS (ESI) (m/z): $[M]^+$ calcd for $C_{32}H_{30}N_2O_4$, 506.23; found, 506.20. Melting Point = 126.1°C. The related Mass and FTIR spectra are shown in Figs. S2 and S5 of the supporting information, respectively.

**(ii) H-acceptor $\mathbf{P_{III}}$.** Compound **2** (2 g, 3.7 mmol), pyridin-3-ol (0.415 g, 4.48 mmol) and DMAP (0.048 g, 0.37 mmol) were dissolved in dry DCM (100 ml) in nitrogen system, then DCC (2.27 g, 11.1 mmol) was added in the solution. The solution was reacted for 16 hours at room temperature. After reaction, the mixture filtrated and then washed with DCM. The solution was extracted with deionized water/DCM, then the organic phase of solution was obtained. The organic phase was dried by $MgSO_4$ and concentrated using a rotary evaporator. The residue was purified by column chromatography on silica (*n*-hexane/DCM = 5:3, v/v). The final product as a white solid has a yield of 57%. $^1$H NMR (300 MHz, $CDCl_3$) δ(ppm): 8.6 (s, 1H, pyridine-H), 8.51 (d, $J$ = 6.2 Hz, 1H, pyridine-H), 8.03 (d, $J$ = 8.1 Hz, 2H, Ar-H), 7.88 (s, 4H, Ar-H), 7,75 (d, $J$ = 7.7 Hz, 2H, Ar-H), 7.70 (d, $J$ = 6.5 Hz, 1H, pyridine-H), 7.50 (d, $J$ = 7.1 Hz, 1H, pyridine-H), 7.16 (d, $J$ = 7.9 Hz, 2H, Ar-H), 7.06 (d, $J$ = 8.2 Hz, 2H, Ar-H), 4.13 (t, $J$ = 8.7 Hz, 4H, -$OCH_2$-), 1.90-1.70 (m, 5H, -$CH_2$-), 1.70-1.45 (m, 2H, -$CH_2$-). Anal. Calcd for $C_{38}H_{32}N_2O_6$: C 74.49, H 5.26, N 4.57; Found: C 74.23, H 5.18, N 4.53. Melting Point = 138.4°C. MS (ESI) (m/z): $[M]^+$ calcd for $C_{38}H_{32}N_2O_6$, 612.67; found, 612.70. The related Mass and FTIR spectra are shown in Figs. S3 and S6 of the supporting information, respectively.

**(iii) H-acceptor $\mathbf{P_{III}}$*.** Compound **3** (2 g, 3.1 mmol), pyridin-3-ol (0.345 g, 3.72 mmol) and DMAP (0.04 g, 0.31 mmol) were dissolved in dry DCM (100 ml) in nitrogen system, then DCC (1.9 g, 9.3 mmol) was added in the solution. The solution was reacted for 16 hours at room temperature. After reaction, the mixture filtrated and then washed with DCM. The solution was extracted with deionized water/DCM, then the organic phase of solution was obtained. The organic phase was dried by $MgSO_4$ and concentrated using a rotary evaporator. The residue was purified by column chromatography on silica (*n*-hexane/DCM = 5:3, v/v). The final product as a white solid has a yield of 59%. $^1$H NMR (300 MHz, $CDCl_3$) δ(ppm): 8.6 (s, 1H, pyridine-H), 8.55 (d, $J$ = 6.6 Hz, 1H, pyridine-H), 8.25 (d, $J$ = 8.2 Hz, 2H, Ar-H), 8.11 (d, $J$ = 7.8 Hz, 2H, Ar-H), 8.00 (d, $J$ = 6.9 Hz, 1H, pyridine-H),7.83 (s, 4H, Ar-H), 7.72 (d, $J$ = 8.0 Hz, 2H, Ar-H), 7.55 (d, $J$ = 7.5 Hz, 1H, pyridine-H), 7.49 (d, $J$ = 8.3 Hz, 2H, Ar-H), 7.15 (d, $J$ = 8.4 Hz, 2H, Ar-H), 7.05 (d, $J$ = 8.3 Hz, 2H, Ar-H), 4.12 (m, 4H, -$OCH_2$-), 1.90-1.70 (m, 5H, -$CH_2$-), 1.71-1.45 (m, 2H, -$CH_2$-), 1.00 (d, $J$ = 8.8 Hz, 3H, -$CH_3$). Anal. Calcd for $C_{39}H_{34}N_2O_6$: C 74.74, H 5.47, N 4.47; Found: C 74.61, H 5.42, N 4.44. MS (ESI) (m/z): $[M]^+$ calcd for $C_{39}H_{34}N_2O_6$, 626.24; found, 626.30. Melting Point = 135.6°C. The related Mass and FTIR spectra are shown in Figs. S4 and S7 of the supporting information, respectively.

**(iv) H-donor $\mathbf{A_{II}F}$*.** Compound **4** (11.25 g, 42 mmol), benzyl 4-hydroxybenzoate (8 g, 35 mmol), and DMAP (0.65 g, 5.3 mmol) were dissolved in dry DCM (250 ml) in nitrogen system, then DCC (14.5 g, 70 mmol) was added in solution. The solution was reacted for 16 hours at room temperature. After reaction, the mixture filtrated and then washed with DCM. The solution was extracted with deionized water/DCM, then the organic phase of solution was obtained. The organic phase was dried by $MgSO_4$ and concentrated using a rotary evaporator. The residue was purified by column chromatography on silica (*n*-hexane/DCM = 5:1, v/v). The intermediate as a light yellow solid (yield: 88%). Then the intermediate (10 g, 20 mmol) and 15% Pd/C (1.5 g) were dissolved in dry THF. The mixed solution was reacted overnight at room temperature upon hydrogen system. After reaction, the solution mixture filtrated and then washed with THF, then concentrated using a rotary evaporator. The residue was recrystallized by *n*-hexane/DCM.

The final product as a white solid has a yield of 94%. $^1$H NMR (300 MHz, $CDCl_3$) δ(ppm): 8.16 (d, *J* = 8.7 Hz, 2H, Ar-H), 8.03 (t, *J* = 8.0 Hz, 1H, Ar-H), 7.32 (m, 2H, Ar-H), 6.74 (dd, *J* = 9.0 Hz, 1H, Ar-H), 6.68 (dd, *J* = 11.7 Hz, 1H, Ar-H), 4.42 (m, 1H, -OCH-), 1.71-1.60 (m, 2H, -$CH_2$-), 1.33-1.27 (m, 11H, -$CH_2CH_3$), 0.86 (t, *J* = 6.3 Hz, 3H, -$CH_3$). Anal. Calcd for $C_{22}H_{25}FO_5$: C 68. 03, H 6.49; Found: C 67.78, H 6.44. Melting Point = 150.1°C. The related information is shown in the literature.[53]

**(v) H-donor $A_{II}$*.** Compound **5** (10.51 g, 42 mmol), benzyl 4-hydroxybenzoate (8 g, 35 mmol) and DMAP (0.65 g, 5.3 mmol) were dissolved in dry DCM (250 ml) in nitrogen system, then DCC (14.5 g, 70 mmol) was added in solution. The solution was reacted for 16 hours at room temperature. After reaction, the mixture filtrated and then washed with DCM. The solution was extracted with deionized water/DCM, then the organic phase of solution was obtained. The organic phase was dried by $MgSO_4$ and concentrated using a rotary evaporator. The residue was purified by column chromatography on silica (*n*-hexane/DCM = 5:1, v/v). The final product as a white solid (yield: 83%). Then the product (7.4 g, 20 mmol) and 15% Pd/C (1.11 g) were dissolved in dry THF. The mixed solution was reacted overnight at room temperature upon hydrogen system. After reaction, the mixture filtrated and then washed with THF, then concentrated using a rotary evaporator. The residue was recrystallized by *n*-hexane/DCM. The final product as a white solid has a yield of 90%. $^1$H NMR (300 MHz, $CDCl_3$) δ(ppm): 8.22-8.14 (m, 4H, Ar-H), 7.33 (d, *J* = 8.4 Hz, 2H, Ar-H), 6.98 (d, *J* = 8.4 Hz, 2H, Ar-H), 4.52 (m, 1H, -OCH), 1.79-1.60 (m, 2H, -$CH_2$), 1.39-1.32 (m, 11H, -$CH_2$), 0.91 (t, *J* = 5.7 Hz, 3H, -$CH_3$). Anal. Calcd for $C_{22}H_{26}O_5$: C 71.33, H, 7.07; Found: C 70.96, H 7.11. Melting Point = 157.3°C. The related information is shown in the literature.[53]

**(vi) H-donor $A_{II}$F.** Compound **6** (10.68 g, 42 mmol), benzyl 4-hydroxybenzoate (8 g, 35 mmol) and DMAP (0.65 g, 5.3 mmol) were dissolved in dry DCM (250 ml) in nitrogen system, then DCC (14.5 g, 70 mmol) was added in solution. The solution was reacted for 16 hours at room temperature. After reaction, the mixture filtrated and then washed with DCM. The solution was extracted with deionized water/DCM, then the organic phase of solution was obtained. The organic phase was dried by $MgSO_4$ and concentrated using a rotary evaporator. The residue was purified by column chromatography on silica (*n*-hexane/DCM = 5:1, v/v). The intermediate as a white solid (yield: 85%). Then the intermediate (10 g, 21.5 mmol) and 15% Pd/C (1.11 g) were dissolved in dry THF. The mixed solution was reacted overnight at room temperature in hydrogen system. After reaction, the mixture filtrated and then washed with THF, then concentrated using a rotary evaporator. The residue was recrystallized by *n*-hexane/DCM. The final product as a white solid has a yield of 91%. $^1$H NMR (300 MHz, $CDCl_3$) δ(ppm): 8.17 (d, *J* = 8.7 Hz, 2H, Ar-H), 8.14 (t, *J* = 8.7 Hz, 1H, Ar-H), 7.32 (d, *J* = 8.7 Hz, 2H, Ar-H), 6.77 (m, 1H, Ar-H), 6.68 (m, 1H, Ar-H), 4.00 (t, *J* = 6.6 Hz, 2H, -$OCH_2$-), 1.86 (t, 2H, -$CH_2$-), 1.47-1.27 (m, 8H, -$CH_2$-), 0.86 (t, *J* = 6.5 Hz, 3H, -$CH_3$). Anal. Calcd for $C_{21}H_{23}FO_5$: C 67.37, H 6.19; Found: C 67.25, H 6.39. Melting Point = 152.8°C. The related information is shown in the literature.[53]

**(vii) H-donor $A_{III}$F*.** Compound **7** (i.e., **AF***) (21.36 g, 42 mmol), benzyl 4-hydroxybenzoate (8 g, 35 mmol), and DMAP (0.65 g, 5.3 mmol) were dissolved in dry DCM (250 ml) in flask with round bottom in nitrogen system, then DCC (14.5 g, 70mmol) was added in solution. The solution was reacted for 16 hours at room temperature. After reaction, the mixture filtrated and then washed with DCM. The solution was extracted with deionized water/DCM, then the organic phase of solution was obtained. The organic phase was dried by $MgSO_4$ and concentrated using a rotary evaporator. The residue was purified by column chromatography on silica (*n*-hexane/DCM = 5:1, v/v). The intermediate as a light yellow solid (yield: 94%). Then the intermediate (15 g, 29.5 mmol) and 15% Pd/C (2.25 g) was dissolved in dry THF. The mixed solution was reacted overnight at room temperature upon hydrogen system. After reaction, the mixture filtrated and then washed with THF, then concentrated using a rotary evaporator. The residue was recrystallized by *n*-hexane/DCM. The final product as a white solid has a yield of 89%. $^1$H NMR (300 MHz, $CDCl_3$) δ(ppm): 8.30 (d, *J* = 8.4 Hz, 2H, Ar-H), 8.20 (d, *J* = 7.8 Hz, 2H, Ar-H), 8.02 (d, *J* = 6.2 Hz, 1H, Ar-H), 7.40 (d, *J* = 8.1 Hz, 2H, Ar-H), 7.31 (d, *J* = 7.9 Hz, 2H, Ar-H), 6.75 (d, *J* = 7.1 Hz, 1H, Ar-H), 4.42 (m, 1H, -OCH-),1.59 (m, 2H, -$CH_2$-), 1.31-1.25 (m, 8H, -$CH_2$-), 0.89 (t, *J* = 5.3 Hz, 3H, -$CH_3$). Anal. Calcd for $C_{29}H_{29}FO_7$: C 68.29, H 5.75; Found: C 67.93, H 5.59. Melting Point = 159.4°C. The related information is shown in the literature.[53]

**(viii) H-donor $A_{II}$.** Compound **8** (8.93 g, 20 mmol) and 15% Pd/C (1.11 g) were dissolved in dry THF. The mixed solution was reacted overnight at room temperature in hydrogen system. After reaction, the solution first through filtration followed by THF washing, then concentrated using a rotary evaporator. The residue was recrystallized by *n*-hexane/DCM. The final product as a white solid (yield: 90%). $^1$H NMR (300 MHz, $CDCl_3$) δ(ppm): 8.05 (m, 4H, Ar-H), 7.35 (d, *J* = 8.4 Hz, 2H, Ar-H), 6.90 (d, *J* = 8.4 Hz, 2H, Ar-H), 4.05 (t, *J* = 6.3 Hz, 2H, -$OCH_2$-), 1.70-1.61 (m, 2H, -$CH_2$-), 0.86 (t, *J* = 6.3 Hz, 3H, -$CH_3$). Anal. Calcd for $C_{21}H_{24}O_5$: C 70.7, H, 6.79; Found: C 70.65, H 6.74. Melting Point = 160.1°C. The related information is shown in the literature.[53]

**Preparation of supramolecular diads C/D (1:1 mol/mol).** All supramolecular diads were constructed by mixing the same molar ratios of H-acceptors **C** ($P_{III}$, $P_{III}$* and $P_{II}$*) and H-donors **D** ($A_{II}$, $A_{II}$*, $A_{II}$F, $A_{II}$F* and $A_{III}$F*) in solutions of chloroform/THF (~3:1 vol), which were self-assembled into supramolecules by evaporating solvents slowly. All H-acceptors **C** were H-bonded with H-donors **D** to form supramolecular diads **C**/**D** in the molar ratio of 1:1.

## Results and discussion

As shown in Fig. 1a, a series of supramolecular diads **C**/**D** (1:1 mol/mol) were prepared by the same molar ratios of various H-acceptors **C** (i.e., proton acceptors **C** = $P_{III}$, $P_{III}$* and $P_{II}$*) and H-donors **D** (i.e., proton donors **D** = $A_{II}$, $A_{II}$*, $A_{II}$F, $A_{II}$F* and

Journal Name

View Article Online
DOI: 10.1039/C6RA19266A



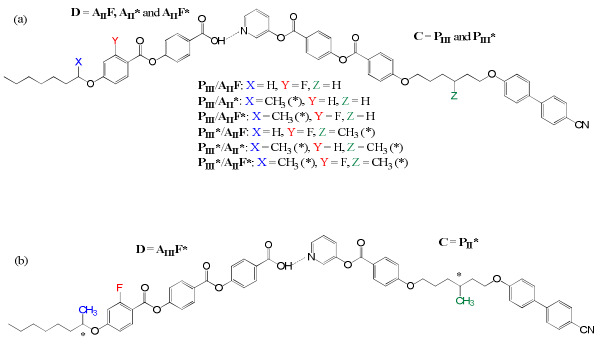


**Fig. 1** Molecular structures of supramolecular diads **C**/**D** (1:1 mol/mol): (a) $\mathbf{P_{III}}/\mathbf{A_{II}F}$, $\mathbf{P_{III}}/\mathbf{A_{II}}$*, $\mathbf{P_{III}}/\mathbf{A_{II}F}$*, $\mathbf{P_{III}}$*/$\mathbf{A_{II}F}$, $\mathbf{P_{III}}$*/$\mathbf{A_{II}}$* and $\mathbf{P_{III}}$*/$\mathbf{A_{II}F}$* and (b) $\mathbf{P_{II}}$*/$\mathbf{A_{III}F}$*.

$\mathbf{A_{III}F}$*), where **P**, Roman numberals, *, **A**, **F**, and denote pyridyl derivatives (H-acceptors), numbers of H-bonded aromatic rings, chiral center, benzoic acid derivatives (H-donors), and lateral fluoride substitution (lateral dipole moment), respectively. The supramolecular diads **C**/**D**, which are formed by two complimentary components between H-acceptors **C** and H-donors **D**, possess CO(OH)···N with a stronger H-bonded interaction than their H-bonded acid dimers.

**Mesophasic properties**

The phase transition temperatures, enthalpies, mesophasic ranges and helical twisting power (HTP) values of all supramolecular diads **C**/**D** (1:1 mol/mol) obtained by DSC and POM are illustrated in Table 1. The various locations of H-bonds and chiral centers, numbers of chiral centers and the lateral fluoride substitution in chemical structures of supramolecular diads **C**/**D** were affected by the liquid crystalline properties of supramolecular diads **C**/**D**, and their individual effects are illustrated as Table 1.

**Table 1** Phase transition temperatures (°C),[a,b] enthalpies (J $g^{-1}$), mesophasic ranges and HTP values ($\mu m^{-1}$) of supramolecular diads **C**/**D** (1:1 mol/mol)

| Diads **C**/**D** (1:1) | Phase transition temperature (°C) and [enthalpies (J $g^{-1}$)] | BP range (°C) | HTP ($\mu m^{-1}$) |
|---|---|---|---|
| $\mathbf{P_{III}}$*/$\mathbf{A_{II}}$ | Iso 146.9 [0.76] N* 96.6 [1.98] SmA 41.3 [1.22] K | -- | 3.1 |
| $\mathbf{P_{III}}$*/$\mathbf{A_{II}F}$ | Iso 145.2 [0.98] N* 88.1 [2.71] SmA 44.9 [3.40] K | -- | 3.4 |
| $\mathbf{P_{III}}/\mathbf{A_{II}}$* | Iso 124.6 [0.44] N* 97.4 [3.01] SmA 56.8 [1.21] K | -- | 3.7 |
| $\mathbf{P_{III}}/\mathbf{A_{II}F}$* | Iso 122.6 [0.46] N* 97.4 [2.67] SmA 64.6 [1.24] K | -- | 3.9 |
| $\mathbf{P_{III}}$*/$\mathbf{A_{II}}$* | Iso 151.2 [0.45] BPI 137.5[c] N* 106.6 [2.02] SmA 68.2 [0.99] K | 13.7 | 4.2 |
| $\mathbf{P_{III}}$*/$\mathbf{A_{II}F}$* | Iso 148.3 [0.67] N* 86.8 [1.87] SmA 60.6 [1.31] K | -- | 4.3 |
| $\mathbf{P_{II}}$*/$\mathbf{A_{III}F}$* | Iso 151.8 [0.73] N* 111.2 [1.98] SmA 86.2 [1.27] K | -- | 4.8 |

*[a]Peak temperatures in the DSC profiles obtained during the first cooling cycles at a rate of 0.5°C/min. [b]Iso = isotropic phase; BPI = blue phase I; N* = cholesteric phase; K = crystalline phase. [c]Phase transition temperatures were obtained by POM and the enthalpy could not be obtain by DSC.

**Effects of various locations of H-bonds on supramolecular diads C/D (i.e., $\mathbf{P_{III}}$*/$\mathbf{A_{II}F}$* and $\mathbf{P_{II}}$*/$\mathbf{A_{III}F}$*)**

The structural effects on the mesophasic properties of analogous supramolecular diads $\mathbf{P_{III}}$*/$\mathbf{A_{II}F}$* and $\mathbf{P_{II}}$*/$\mathbf{A_{III}F}$* with different locations of H-bonds in H-bonded bent-core mesogen were compared. As shown in Fig. 2, the supramolecular diad $\mathbf{P_{III}}$*/$\mathbf{A_{II}F}$* ($\Delta T_{N*}$ = 62.8°C) with more symmetric H-bonded bent-core structure has a wider cholesteric phase range than its analogous supramolecular diad $\mathbf{P_{II}}$*/$\mathbf{A_{III}F}$* ($\Delta T_{N*}$ = 40.6°C), but both with a similar smectic A phase range. Moreover, both cholesteric and smectic A phases were obtained at lower transition temperatures upon cooling ($T_{Iso\text{-}N*}$ = 148.3°C, $T_{N*\text{-}SmA}$ = 86.8°C and $T_{SmA\text{-}K}$ = 60.6°C) in $\mathbf{P_{III}}$*/$\mathbf{A_{II}F}$*. Therefore, the wider cholesteric phase range and lower phase transition temperatures are obtained in $\mathbf{P_{III}}$*/$\mathbf{A_{II}F}$* with a more symmetric H-bonded bent-core structure. The narrower cholesteric phase range of supramolecular diad $\mathbf{P_{II}}$*/$\mathbf{A_{III}F}$* might be related to its large HTP value of 4.8 $\mu m^{-1}$ in contrast to a proper HTP value of 4.3 $\mu m^{-1}$ in $\mathbf{P_{III}}$*/$\mathbf{A_{II}F}$*.

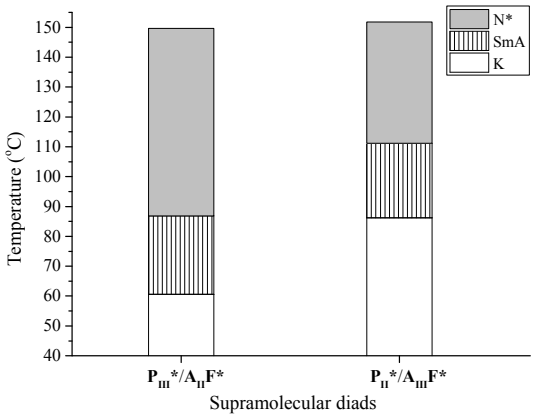


**Fig. 2** Mesophases and temperature ranges of analogous supramolecular diads $\mathbf{P_{III}}$*/$\mathbf{A_{II}F}$* and $\mathbf{P_{II}}$*/$\mathbf{A_{III}F}$* upon cooling.

**Effects of various numbers and locations of chiral centers on supramolecular diads C/D (i.e., $\mathbf{P_{III}}$*/$\mathbf{A_{II}F}$, $\mathbf{P_{III}}$*/$\mathbf{A_{II}F}$*and $\mathbf{P_{III}}/\mathbf{A_{II}F}$*)**

As shown in Fig. 3, analogous supramolecular diads $\mathbf{P_{III}}$*/$\mathbf{A_{II}F}$, $\mathbf{P_{III}}$*/$\mathbf{A_{II}F}$* and $\mathbf{P_{III}}/\mathbf{A_{II}F}$* possess similar chemical structures with different locations and numbers of chiral centers on these diads, where chiral centers are on H-acceptor of $\mathbf{P_{III}}$*/$\mathbf{A_{II}F}$, both H-acceptor/H-donor of $\mathbf{P_{III}}$*/$\mathbf{A_{II}F}$* and H-donor of $\mathbf{P_{III}}/\mathbf{A_{II}F}$*. Among these supramolecular diads, $\mathbf{P_{III}}$*/$\mathbf{A_{II}F}$* has the widest cholesteric phase ($\Delta T_{N*}$ = 62.8°C), which is wider than $\mathbf{P_{III}}$*/$\mathbf{A_{II}F}$ ($\Delta T_{N*}$ = 57.2°C) and $\mathbf{P_{III}}/\mathbf{A_{II}F}$* ($\Delta T_{N*}$ = 25.2°C). Therefore, the cholesteric phase of supramolecular diad $\mathbf{P_{III}}$*/$\mathbf{A_{II}F}$* was stabilized by introducing double chiral centers on both H-acceptor and H-donor. On the other hand, $\mathbf{P_{III}}$*/$\mathbf{A_{II}F}$* has the narrowest smectic A phase range $\Delta T_{SmA}$ = 26.2°C (vs. 32.8°C in $\mathbf{P_{III}}/\mathbf{A_{II}F}$* and 43.2°C in $\mathbf{P_{III}}$*/$\mathbf{A_{II}F}$) upon cooling. According to these mesophase ranges and phase transition temperatures, we can summarize some results of the chiral center effects on supramolecular diads: (a) Double chiral centers (i.e., $\mathbf{P_{III}}$*/$\mathbf{A_{II}F}$*): the cholesteric phase was easily stabilized (the widest cholesteric range) by introducing both

View Article Online
DOI: 10.1039/C6RA19268A
Journal Name



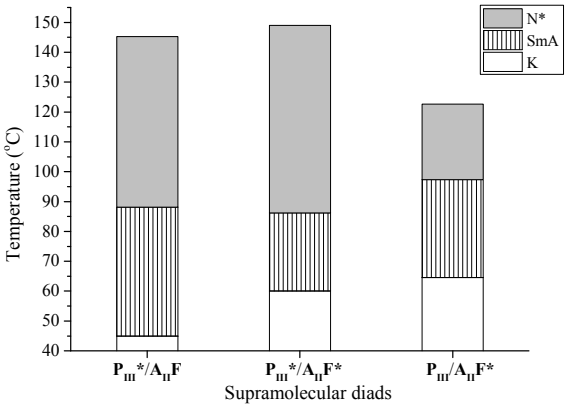


**Fig. 3** Mesophases and temperature ranges of analogous supramolecular diads $\mathbf{P_{III}*/A_{II}F}$, $\mathbf{P_{III}*/A_{II}F*}$ and $\mathbf{P_{III}/A_{II}F*}$ upon cooling.

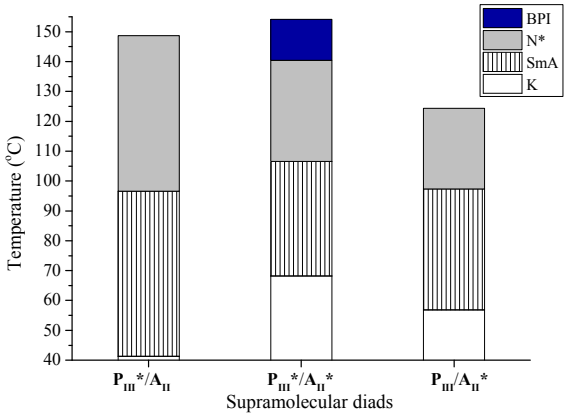


**Fig. 4** Mesophases and temperature ranges of analogous supramolecular diads $\mathbf{P_{III}*/A_{II}}$, $\mathbf{P_{III}*/A_{II}*}$ and $\mathbf{P_{III}/A_{II}*}$ upon cooling.

chiral centers to H-acceptor and H-donor of supramolecular diad $\mathbf{P_{III}*/A_{II}F*}$ (upon cooling) due to its stronger helical twisting power HTP = 4.3 $\mu m^{-1}$ (vs. 3.9 $\mu m^{-1}$ of $\mathbf{P_{III}/A_{II}F*}$ and 3.4 $\mu m^{-1}$ of $\mathbf{P_{III}*/A_{II}F}$, see Table 1). In other words, the introduction of dual-chiral centers (on both H-acceptor and H-donor) to supramolecular diad $\mathbf{P_{III}*/A_{II}F*}$ also hindered the smectic A phase formation (with the narrowest smectic A phase range $\Delta T_{SmA}$ = 26.2°C) due to its looser staking. (b) Single chiral center (i.e., $\mathbf{P_{III}*/A_{II}F}$ and $\mathbf{P_{III}/A_{II}F*}$): The mesophase ranges and phase transition temperatures of supramolecular diads are affected by the locations of the chiral center (on H-acceptor or H-donor). The smallest HTP value was obtained in supramolecular diad $\mathbf{P_{III}*/A_{II}F}$ due to the chiral center on the flexible spacer. Thus, we can presume that the smallest HTP value of supramolecular diad $\mathbf{P_{III}*/A_{II}F}$ might induce a better stacking, where the smectic A phases could be stabilized to have the broadest range $\Delta T_{SmA}$ = 43.2°C. The induced effects of HTP values in supramolecular diads with a single chiral center were different from the result with dual-chiral centers, due to the three-dimensional spatial arrangements of supramolecular diads. The mesophase ranges of the supramolecular diads containing rod-like and H-bonded bent-core mesogens with different locations and numbers of chiral centers are similar to our published results of H-bonded dimeric liquid crystals containing two rod-like mesogens.[70]

**Effects of no lateral fluoride substitution on supramolecular diads C/D (i.e., $\mathbf{P_{III}*/A_{II}}$, $\mathbf{P_{III}*/A_{II}*}$ and $\mathbf{P_{III}*/A_{II}}$)**

As shown in Fig. 4, analogous supramolecular diads $\mathbf{P_{III}*/A_{II}}$, $\mathbf{P_{III}*/A_{II}*}$ and $\mathbf{P_{III}/A_{II}*}$ without lateral fluoride substitution possess similar chemical structures with different locations and numbers of chiral centers on these diads, where chiral centers are on H-acceptor of $\mathbf{P_{III}*/A_{II}}$, both H-acceptor/H-donor of $\mathbf{P_{III}*/A_{II}*}$ and H-donor of $\mathbf{P_{III}/A_{II}*}$. Among these supramolecular diads, $\mathbf{P_{III}*/A_{II}}$ has the widest cholesteric phase range $\Delta T_{N*}$ = 52.1°C (vs. 33.8°C in $\mathbf{P_{III}*/A_{II}*}$ and 27°C in $\mathbf{P_{III}/A_{II}*}$) upon cooling, but $\mathbf{P_{III}/A_{II}*}$ with a chiral center on H-donor has the narrowest $\Delta T_{N*}$ = 27°C. Similar to supramolecular diads with lateral fluoride substitution, $\mathbf{P_{III}*/A_{II}*}$ has the narrowest smectic A phase range $\Delta T_{SmA}$ = 38.4°C (vs. 40.6°C in $\mathbf{P_{III}/A_{II}*}$ and 55.3°C in $\mathbf{P_{III}*/A_{II}}$) upon cooling. According to Figs. 3 and 4, the corresponding supramolecular diads with lateral fluoride substitution (i.e., $\mathbf{P_{III}*/A_{II}F}$, $\mathbf{P_{III}*/A_{II}F*}$ and $\mathbf{P_{III}/A_{II}F*}$) were compared with those without lateral fluoride substitution (i.e., $\mathbf{P_{III}*/A_{II}}$, $\mathbf{P_{III}*/A_{II}*}$ and $\mathbf{P_{III}/A_{II}*}$) to investigate the fluoride effects on supramolecular diads. Based on the mesophase ranges and phase transition temperatures, we can summarize some results of chiral center effects on supramolecular diads: (a) Double chiral centers (i.e., $\mathbf{P_{III}*/A_{II}*}$): The blue phase I (i.e., BPI) was induced by the removal of lateral fluoride substitution in supramolecular diad $\mathbf{P_{III}*/A_{II}*}$ (in contrast to $\mathbf{P_{III}*/A_{II}F*}$ with lateral fluoride substitution), which will be further explained in the theoretical simulation. (b) No lateral fluoride substitution: In comparison with their corresponding supramolecular diads with lateral fluoride substitution, all supramolecular diads $\mathbf{P_{III}*/A_{II}}$, $\mathbf{P_{III}*/A_{II}*}$ and $\mathbf{P_{III}*/A_{II}}$ without lateral fluoride substitution have lower HTP values and smaller dipole moments to induce lower phase transition temperatures (even with similar phase sequences, except the blue phase of $\mathbf{P_{III}*/A_{II}*}$). In contrast to supramolecular diads $\mathbf{P_{III}*/A_{II}}$ and $\mathbf{P_{III}/A_{II}}$*s with single chiral center, the BPI was introduced in supramolecular diad $\mathbf{P_{III}*/A_{II}*}$ with dual-chiral centers due to its stronger helical twisting power HTP = 4.2 $\mu m^{-1}$ (vs.3.7 $\mu m^{-1}$ of $\mathbf{P_{III}/A_{II}*}$ and 3.1 $\mu m^{-1}$ of $\mathbf{P_{III}*/A_{II}}$, see Table 1).

**Effects of molar ratios of H-acceptor/H-donor on BPI of supramolecular diad $\mathbf{P_{III}*/A_{II}*}$**

Normally, supramolecular diads are prepared by self-assembly of the same molar ratio of H-acceptors and H-donors. However, the supramolecular complexes are generated by over-supplies of H-donors to have the mixtures of supramolecular diads (H-acceptor/H-donor=1:1 mol/mol) and H-bonded acid dimers (excessive H-donors with acid groups). Due to the introduction of the second mesogenic cores by H-bonded acid dimmers, the

View Article Online
DOI: 10.1039/C6RA19266A ARTICLE



blue phase ranges of supramolecular complexes by over-supplies of H-donors are usually wider than those of supramolecular diads in some previous published results.[42,67] Moreover, the optimal molar ratio of supramolecular complexes with the widest blue phase ranges is around H-acceptor/H-donor=1:3, which has an equal molar ratio of supramolecular diads and H-bonded acid dimmers. In general, the linear acid dimers have high compatibilities with linear supramolecular diads and the mesophases of acid dimers will not seriously affect the blue phases of the supramolecular diads. Hence, the blue phase ranges of supramolecular complexes $P_{III}$*/$A_{II}$* (i.e., $A_{II}$*=45-75 mol%) are compared with that of supramolecular diad $P_{III}$*/$A_{II}$* (i.e., $A_{II}$*=50 mol%) in Fig. 5. The BPI was completely destroyed by the excessive addition of H-acceptor $P_{III}$* in supramolecular complex $P_{III}$*/$A_{II}$* (i.e., $A_{II}$*=45 mol%), and it revealed an unfavorable trend by the excessive addition of acid dimer (till the disappearance of the BPI at $A_{II}$*=70 mol%) and the detailed information of phase transition temperatures and enthalpies are shown in Table S1. These reductions of the BPI ranges in supramolecular complexes $P_{III}$*/$A_{II}$* (i.e., $A_{II}$*=50-75 mol%) with over-supplies of H-donors (0-25 mol% to form acid dimer) are originated from the poor miscibilities between linear acid dimer and supramolecular diad $P_{III}$*/$A_{II}$* (i.e., $A_{II}$*=50 mol%) with H-bonded bent-core due to their shape variations. In most previous cases, the widest blue phase ranges of supramolecular complexes were obtained by adding 75 mol% of H-donors (i.e., H-accepter/H-donor=1:3). However, in this study the widest blue phase range of this supramolecular complexes $P_{III}$*/$A_{II}$* was obtained in adding 50 mol% of H-donor $A_{II}$* (i.e., H-accepter/H-donor=1:1). Finally, we found that the special optimal 1:1 molar ratio of supramolecular diad $P_{III}$*/$A_{II}$* (i.e., H-donor=50 mol%) with the widest blue phase range is mainly attributed to its rod-like and H-bonded bent-core mesogens, rather than H-donor=75 mol% in most supramolecular complexes containing linear H-bonded rod-like mesogens.

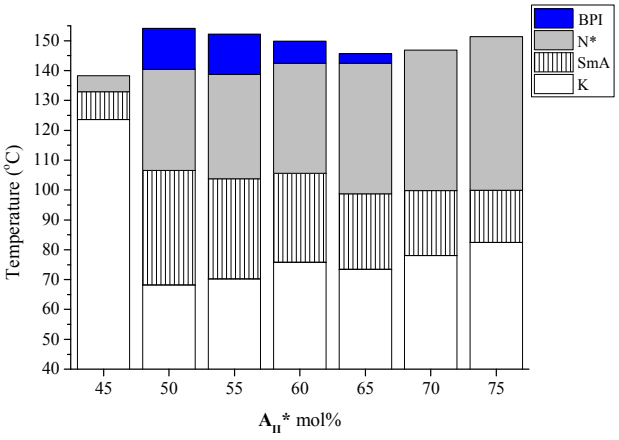


**Fig. 5** Mesophases and temperature ranges of supramolecular complexes **$P_{III}$*/$A_{II}$*** with various molar ratio of H-donor **$A_{II}$*** upon cooling.

**Theoretical simulation**

The mesophasic properties of supramolecular diads, especially the widest blue phase range of 13.7°C in supramolecular diad **$P_{III}$*/$A_{II}$*** = 1:1 mol/mol, could not be completely analyzed by the results of DSC and POM experiments, so we further investigated the related mesomorphic properties by the molecular modeling. The factors like biaxial parameters $W_1/W_2$, bent angles (°), dipole moments (Debye) of the supramolecualr diads might play important roles in the stabilization of BPs, a series of detailed quantum chemical calculation of previous parameters and charge density distribution properties of supramolecular diads **C/D** (i.e., **$P_{III}$*/$A_{II}$**, **$P_{III}$*/$A_{II}$F**, **$P_{III}$/$A_{II}$***, **$P_{III}$/$A_{II}$F***, **$P_{III}$*/$A_{II}$***, **$P_{III}$*/$A_{II}$F*** and **$P_{II}$*/$A_{III}$F***) are shown in Table 2, where these parameters are defined as follows: $W_1$ = width along the short axis normal to the benzene plane and $W_2$ = width along the short axis parallel to the benzene plane; dipole moment D = the measure of the electrical polarity of a molecule of charges and bent angle = the angle between the center of the first, central and final benzene rings of the bent-core structure. In addition, the calculated H-bond lengths in all diads were similar to each other ca. 1.7 Å. Moreover, the detail information (i.e., the optimized geometries and electronic optimization) of all supramolecular diads **C/D** (i.e., **$P_{III}$*/$A_{II}$**, **$P_{III}$*/$A_{II}$F**, **$P_{III}$/$A_{II}$***, **$P_{III}$/$A_{II}$F***, **$P_{III}$*/$A_{II}$***, **$P_{III}$*/$A_{II}$F*** and **$P_{II}$*/$A_{III}$F***) are summarized in Fig. S1.

**Table 2** Calculated bend angles (°), biaxial paremeters, dipole moments (Debye) and HTP ($\mu m^{-1}$) of optimized supramolecular diads **C/D** = 1:1 mol/mol at the B97D/6-31G(d,p) level

| Diads **C/D** (1:1 mol/mol) | Bent angle (°) | Biaxial parameter ($W_1/W_2$) | Dipole moment (Debye) | HTP ($\mu m^{-1}$) |
|---|---|---|---|---|
| **$P_{III}$*/$A_{II}$** | 125.1 | 2.7 | 3.0 | 3.1 |
| **$P_{III}$*/$A_{II}$F** | 124.6 | 2.6 | 3.9 | 3.4 |
| **$P_{III}$/$A_{II}$*** | 126.4 | 2.8 | 2.6 | 3.7 |
| **$P_{III}$/$A_{II}$F*** | 125.5 | 2.7 | 2.9 | 3.9 |
| **$P_{III}$*/$A_{II}$*** | 127.8 | 3.2 | 3.0 | 4.2 |
| **$P_{III}$*/$A_{II}$F*** | 126.9 | 2.9 | 3.9 | 4.3 |
| **$P_{II}$*/$A_{III}$F*** | 132.7 | 3.1 | 6.8 | 4.8 |

The effects of various numbers and locations of chiral centers on supramolecular diads **C/D** (i.e., **$P_{III}$*/$A_{II}$F**, **$P_{III}$*/$A_{II}$F***, **$P_{III}$/$A_{II}$F*** and **$P_{II}$*/$A_{III}$F***) are compared in Table 2. Among these supramolecular diads, the supramolecular diad **$P_{III}$*/$A_{II}$F*** with two chiral centers on both H-acceptor **$P_{III}$*** and H-donor **$A_{II}$F*** has larger bent angle = 126.9°, biaxial parameter $W_1/W_2$ = 2.9 and HTP = 4.3 $\mu m^{-1}$ than the other two analogous supramolecular diads **$P_{III}$/$A_{II}$F*** (bent angle = 125.5°, $W_1/W_2$ = 2.7 and HTP = 3.9 $\mu m^{-1}$) with one chiral center on H-donor **$A_{II}$F*** and **$P_{III}$*/$A_{II}$F** (bent angle = 124.6°, $W_1/W_2$ = 2.6 and HTP = 3.4 $\mu m^{-1}$) with one chiral center on H-acceptor **$P_{III}$***. Moreover, the dipole moments of supramolecular diads **$P_{III}$*/$A_{II}$F*** (dipole moment = 3.9 Debye) and **$P_{III}$*/$A_{II}$F** are the same, but this value is larger than the dipole moment of supramolecular diad **$P_{III}$/$A_{II}$F*** (dipole moment = 2.9 Debye). In addition, supramolecular diad **$P_{II}$*/$A_{III}$F*** with an asymmetrical H-

View Article Online
DOI: 10.1039/C6RA19268A Journal Name



bonded bent core structure has the largest bent angle = 132.7°, dipole moment = 6.8 Debye and HTP = 4.8 $\mu m^{-1}$ among all analogous supramolecular daids, but the biaxial parameter = 3.1 was smaller than supramolecular diad **$P_{III}$*/$A_{II}$F*** with a symmetrical H-bonded bent core structure.

The effects of lateral fluoride substitution on supramolecular diads **C/D** (i.e., **$P_{III}$*/$A_{II}$**, **$P_{III}$*/$A_{II}$*** and **$P_{III}$*/$A_{II}$**) are also evaluated in Table 2. Similar to supramolecular diads with lateral fluoride substitution, supramolecular diad **$P_{III}$*/$A_{II}$*** with two chiral centers on both H-acceptor **$P_{III}$*** and H-donor **$A_{II}$*** has larger bent angle = 127.8°, biaxial parameter $W_1/W_2$ = 3.2 and HTP = 4.2 $\mu m^{-1}$ than the other two analogous supramolecular diads **$P_{III}$/$A_{II}$*** (bent angle = 126.4°, $W_1/W_2$ = 2.8 and HTP = 3.7 $\mu m^{-1}$) with one chiral center on H-donor **$A_{II}$*** and **$P_{III}$*/$A_{II}$** (bent angle = 125.1°, $W_1/W_2$ = 2.7 and HTP = 3.1 $\mu m^{-1}$) with one chiral center on H-acceptor **$P_{III}$***. Moreover, the dipole moments of supramolecular diads **$P_{III}$*/$A_{II}$*** (dipole moment = 3.0 Debye) and **$P_{III}$*/$A_{II}$** are the same, but this value is larger than the dipole moment of supramolecular diad **$P_{III}$/$A_{II}$*** (dipole moment = 2.6 Debye). The corresponding supramolecular diads with lateral fluoride substitution (i.e., **$P_{III}$*/$A_{II}$F**, **$P_{III}$*/$A_{II}$F*** and **$P_{III}$/$A_{II}$F***) were compared with those without lateral fluoride substitution (i.e., **$P_{III}$*/$A_{II}$**, **$P_{III}$*/$A_{II}$*** and **$P_{III}$/$A_{II}$***) to investigate the fluoride effects on supramolecular diads. Not only larger bent angles and biaxial parameters but also smaller dipole moments and HTP values were obtained by removing the lateral fluoride substitution on supramolecular diads.

In summary, we can generalize the major factors of blue phase formation as follows: The blue phase formation in supramolecular diads was induced by the large biaxial parameter, and the blue phase was only formed in supramolecular diad **$P_{III}$*/$A_{II}$*** which has the largest biaxial parameter ($W_1/W_2$ = 3.2) than the other supramolecular diads. The biaxial parameters of supramolecular diads were increased by larger bent angles of supramolecular diads (except for **$P_{II}$*/$A_{III}$F*** with an asymmetrical H-bonded bent core structure). The larger biaxial parameters ($W_1/W_2$) of supramolecular diads were obtained by removing the lateral fluoride substitution (with smaller dipole moments) on supramolecular diads. Moreover, the larger HTP values of supramolecular diads are easier to stabilize the cholesteric phase in supramolecular diads (except for **$P_{II}$*/$A_{III}$F*** with an asymmetrical H-bonded bent core structure). Therefore, the mesophasic properties of supramolecular diads were not directly affected by the dipole moment values of supramolecular diads, but the larger biaxial parameter (≥ 3.2) and appropriate bent angle (127.8°~132.7°) and HTP value (4.2~4.8$\mu m^{-1}$) of supramolecular diad are easier to induce and stabilize the blue phase.

**Characterization of H-bonded structure in supramolecular diad**

As shown in Fig. 6, H-bonds could be generated by the carboxylic acid of H-donor and the pyridyl group of H-acceptor. The stability of H-bond in suprmolecular diad **$P_{III}$*/$A_{II}$*** (1:1 mol/mol) could be directly confirmed from temperature- dependent FTIR spectra. The appearance of two peaks centered

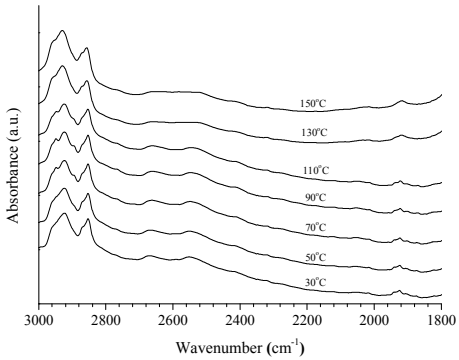


**Fig. 6** Temperature dependent FTIR spectra of supramolecualr diad **$P_{III}$*/$A_{II}$*** (1:1 mol/mol).

at 2552 and 1927 $cm^{-1}$, resulted from the formation of H-bond between carboxylic acid and pyridyl groups (–O–H···N).[68] These intensities of H-bonded characteristic peaks changed smaller but still existed upon heating within 150°C. Thus, supramolecualr diad **$P_{III}$*/$A_{II}$*** was identified to be formed by supramolecular force of intermolecular H-bond, and changes of H-bonded characteristic peaks indicated that the good stability of this strong H-bond in the supramolecualr diad at temperature changes within 150°C.

**Optical and UV-vis investigations of supramolecular diads**

The POM photo images of different phases in supramolecular diads **$P_{III}$*/$A_{II}$*** and **$P_{III}$*/$A_{II}$F*** (1:1 mol/mol) at different temperatures upon cooling are shown in Figs. 7(a)-7(c) and 7(d)-7(e), respectively. Figs. 7(a)-7(c) correspondingly illustrate the blue phase I (PBI) with the platelet texture, the chiral nematic phase (N*) with the Grandjean texture and the chiral smectic A phase (SmA) with the fan-shaped texture.

Moreover, Figs. 7(d)-7(e) also demonstrate correspondent N* and SmA phases. The SmA phase was verified not only by the POM textures but also further by the results of X-ray diffraction (XRD) patterns. In Table S2, the *d*-spacing values of the smectic phase in supramolecular diads were slightly larger than the theoretical molecular lengths of suprmolecular diads. Therefore, the smectic phase of this supramolecular diads was defined as the smectic A phase upon cooling.

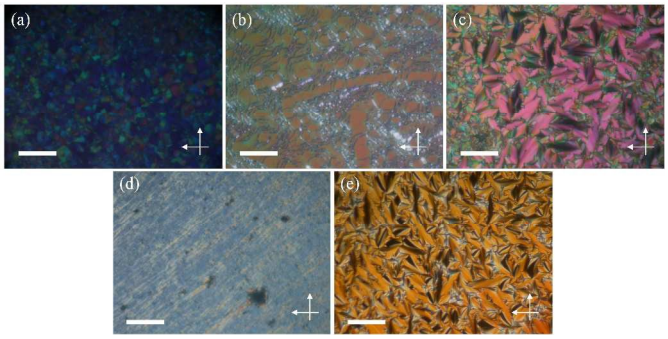


**Fig. 7** POM textures of different phases in supramolecular diads **$P_{III}$*/$A_{II}$*** = 1:1 mol/mol at (a) 145°C, (b) 122°C and (c) 87°C; and

View Article Online
DOI: 10.1039/C6RA19266A ARTICLE



**$P_{III}$*/$A_{II}$F*** = 1:1 mol/mol at (d) 118°C and (e) 74°C upon cooling. (Scale bar: 40 μm, white arrows are the directions of polarizers and analyzers).

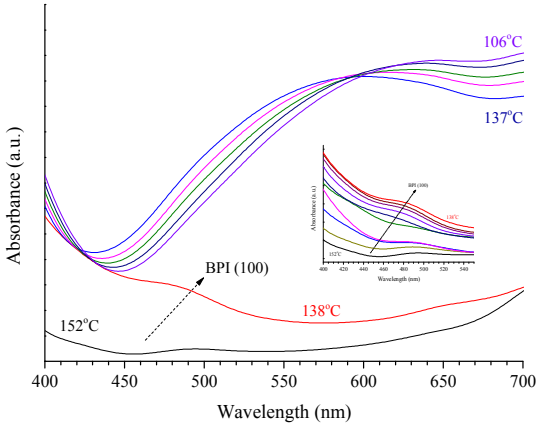


**Fig. 8** Absorbance versus temperature and wavelength of supramolecualr diad **$P_{III}$*/$A_{II}$*** = 1:1 (mol/mol) upon cooling: (a) (110) absorbance of blue phase I (BPI); (b) selective absorbance of the cholesteric phase (N*).

As shown in Fig. 8, the absorbance spectra of supramolecualr diad **$P_{III}$*/$A_{II}$*** = 1:1 (mol/mol) were obtained at different temperatures upon cooling (cooling rate = 0.5 °C/min). The mesophases of supramolecualr diad **$P_{III}$*/$A_{II}$*** = 1:1 (mol/mol) were LC phases (the isotropic, BPI and cholesteric phases) between 151.2°C and 137.5°C upon cooling. Practically, the absorbance peaks of LC phases (i.e., BPI and N*) in the H-bonded bent-core diad **$P_{III}$*/$A_{II}$*** = 1:1 (mol/mol) were reflected away by the special pitch values of the BPI or cholesteric phases at different temperatures. There were no obvious absorbance peaks in supramolecular diad **$P_{III}$*/$A_{II}$*** = 1:1 (mol/mol), due to the isotropic phase at high temperature (152°C). However, a specific absorbance peak ca. 483.5 nm is assigned to the Bragg diffraction[42] from the 110 plane of the cubic lattice in the BPI of supramolecular diad **$P_{III}$*/$A_{II}$*** = 1:1 (mol/mol) by decreasing temperatures to the range of 151-138°C, which are matchable with the BPI observed by POM at 145°C (see Fig. 7a) upon cooling. Moreover, the absorbance peak of the BPI was replaced with the chiral nematic phase with a broader absorbance peak (ca. 601 nm) by decreasing the temperature from 137°C to 106°C, which were correspondent to the selective diffraction of the cholesteric phase. The broader absorbance peak was red-shifted in the cholesteric phase and the pitch was extended by decreasing temperature. A platelet texture of the cholesteric phase was also observed by POM at 122°C upon cooling (see Fig. 7b) which is matchable with the temperature range of 137-106°C. Therefore, the BPI range (151-138°C upon cooling) of supramolecular diad **$P_{III}$*/$A_{II}$*** = 1:1 (mol/mol) was proven not only by the UV-vis spectral changes but also by the characterization of POM textures.

## Conclusions

Several novel supramolecular diads were prepared by self-assembly of H-acceptors (**C** = **$P_{III}$***, **$P_{III}$** and **$P_{II}$***) and H-donors (**D** = **$A_{II}$**, **$A_{II}$F**, **$A_{II}$***, **$A_{II}$F***, and **$A_{III}$F***) to form **C**/**D** = 1:1 mol/mol. Not only the locations and numbers of H-bonds and chiral centers but also the lateral fluoride substitution play the important role for mesophasic properties, especially for the blue phase. The widest cholesteric phase ranges along with the narrowest smectic A phase ranges were obtained in **$P_{III}$*/$A_{II}$*** and **$P_{III}$*/$A_{II}$F*** by introducing two chiral centers on both H-acceptors and H-donors. A proper HTP value of 4.3 $\mu m^{-1}$ in **$P_{III}$*/$A_{II}$F*** with a symmetrical H-bonded bent core structure induced a wider cholesteric phase range than supramolecular diad **$P_{II}$*/$A_{III}$F*** with an asymmetrical H-bonded bent core structure and a larger HTP value of 4.8 $\mu m^{-1}$. Compared with lateral fluoride substitution, all supramolecular diads without fluoride have lower HTP values and smaller dipole moments to induce lower phase transition temperatures. Not only larger bent angles and biaxial parameters but also smaller dipole moments and HTP values were obtained by removing the lateral fluoride substitution on supramolecular diads to achieve the blue phase of **$P_{III}$*/$A_{II}$*** (without lateral fluoride substitution). Surprisingly, the special optimal molar ratio of supramolecular diad **$P_{III}$*/$A_{II}$*** at H-acceptor/H-donor=1:1 (i.e., **$A_{II}$***=50 mol%) with the widest blue phase range is mainly attributed to its rod-like and H-bonded bent-core mesogens, rather than the optimal molar ratio of supramolecular complexes at H-acceptor/H-donor=1:3 (i.e., H-donor=75 mol%) with the widest blue phase ranges in most supramolecular complexes with linear H-bonded rod-like mesogens. Among all supramolecular diads, only supramolecular diad **$P_{III}$*/$A_{II}$*** revealed the blue phase, which possessed an appropriate HTP value (4.2~4.8 $\mu m^{-1}$) and a larger biaxial parameter (≥ 3.2) to stabilize the blue phase in supramolecular diads.

## Acknowledgements

The financial supports of this project are provided by the Ministry of Science and Technology (MOST) in Taiwan through MOST 103-2113-M-009-018-MY3 and MOST 103-2221-E-009-215-MY3.

## Notes and references

Department of Materials Science and Engineering, National Chiao Tung University. 1001 University Road, Hsinchu, Taiwan 300, ROC.

1 I. Fischer, N. Shah and A. Rosch, *Phys. Rev. B* 2008, **77**, 024415.
2 A. Yoshizawa, *RSC Adv*., 2013, **3**, 25475-25497.
3 S. Taushanoff, K. V. Le, J. Williams, R. J. Twieg, B. K. Sadashiva, H. Takezoe and A. Jakli, *J. Mater. Chem.,* 2010, **20**, 5893-5898.
4 I. H. Chiang, C. J. Long, H. C. Lin, W. T. Chuang, J. J. Lee and H. C. Lin, *ACS Appl. Mater. Interfaces* 2014, **6**, 228-235.
5 S. Meiboom, J. p. Sethna, P. W. Anderson and W. F. Brinkma, *Phys. Rev. Lett.,* 1981, **46**, 1216-1219.
6 Z. Zheng, D. Shen and P. Huang, *New J. Phys.*, 2010, **12**, 113018-10.
7 W. Kossel, V. Loeck and H. Z. Voges, *A: Hadrons Nucl.* 1935, **94**, 139.
8 R. J. Miller, H. F. Gleeson and J. E. Lydon, *Phys. Rev. Lett.* 1996, **77**, 857-860.

View Article Online
DOI: 10.1039/C6RA19268A Journal Name




**9** R. M. Hornreich and S. Shtrikman, *Phys. Rev. A* 1981, **24**, 635-638.

**10** L. Longa, D. Monselesan and H. R. Trebin, *Liq. Cryst.* 1989, **5**, 889-898.

**11** P. Pieranski, R. B. Massin and P. E. Cladis, *Phys. Rev. A* 1985, **31**, 3912-3923.

**12** O. Henrich, K. Stratford, M. E. Cates and D. Marenduzzo, *Phys. Rev. Lett.* 2011, **106**, No. 107801.

**13** A. Yoshizawa, M. Kamiyama and T. Hirose, *Appl. Phys. Express* 2011, **4**, No. 101701.

**14** Y. F. Lan, C. Y. Tsai, J. K. Lu and N. Sugiura, *Opt. Express*, 2013, **21**, 5035-5040.

**15** S. Meiboom and M. Sammon, *Phys. Rev. Lett*. 1980, **44**, 882-885.

**16** M. Sato and A. Yoshizawa, *Adv. Mater.* 2007, **19**, 4145-4148.

**17** L. Rao, Z. Ge and S. T. Wu, *Opt. Express* 2010, **18**, 3143-3148.

**18** J. Yan, S. T. Wu, K. L. Cheng and J. W. Shiu, *Appl. Phys. Lett.* 2013, **102**, No. 081102.

**19** W. Cao, A. Munoz, P. P. Muhoray and B. Taheri, *Nat. Mater.* 2002, **1**, 111-113.

**20** K. Higashiguchi, K. Yasui and H. kikuchi, *J. Am. Chem. Soc.* 2008, **130**, 6326-6327.

**21** K. Kim, S. T. Hur, S. Kim, S. Y. Jo, B. R. Lee, M. H. Song and S. W. Choi, *J. Mater. Chem. C*, 2015, **3**, 5383-5388.

**22** C. Y. Huang, J. J. Stott and R. G. Petschek, *Phys. Rev. Lett*. 1998, **80**, 5603-5606.

**23** H. Y. Liu, C. T. Wang, C. Y. Hsu, T. H. Lin and J. H. Liu, *Appl. Phys. Lett.* 2010, **96**, No. 121103.

**24** F. Castles, F. V. Day, S. M. Morris, D. H. Ko, D. J. Gardiner, M. M. Qasim, S. Noheen, P. J. W. Hands, S. S. Choi, R. H. Friend and H. J. Coles, *Nat. Mater.* 2012, **11**, 599-603.

**25** P. P. Crooker in *Chirality in Liquid Crystals* (Eds.: H. S. Kitzerow, C. Bahr), Springer, **2001**, PP. 186-222.

**26** B. Y. Zhang, F. B. Meng and Y. H. Cong, *Opt. Express* 2007, **15**, 10175-10181.

**27** H. Kikuchi, M. Yokota, Y. Hisakado, H. Yang and T. Kajiyama, *Nat. Mater.* 2002, **1**, 64-68.

**28** L. Rao, J. Yan, S. T. Wu, S. I. Yamamoto and Y. Haseba, *Appl. Phys. Lett*. 2011, **98**, No. 081109.

**29** J. Yan and S. T. Wu, *Opt. Mater. Express* 2011, **1**, 1527-1535.

**30** F. Peng, Y. Chen, J. Yuan, H. Chen, S. T. Wu and Y. Haseba, *J. Mater. Chem. C* 2014, **2**, 3597-3601.

**31** H. Yoshida, Y. Tanaka, K. Kawamoto, H. Kubo, T. Tsuda, A. Fujii, S. Kuwabata, H. Kikuchi and M. Ozaki, *Appl. Phys. Express* 2009, **2**, No. 121501.

**32** L. Wang, W. He, Q. Wang, M. Yu, X. Xiao, Y. Zhang, M. Ellahi, D. Zhao, H. Yang and L. Guo, *J. Mater. Chem. C*, 2013, **1**, 6526-6531.

**33** A. Chanishvili, G. Chilaya, G. Petriashvili and P. Collings, *J. Phys. Rev. E* 2005, **71**, No. 51705.

**34** Q. Jin, D. Fu, J. Wei, H. Yang and J. Guo, *RSC Adv.*, 2014, **4**, 28597-28600.

**35** J. Wamg, Y. Shi, K. Yang, J. Wei and J. Guo, *RSC Adv*., 2015, **5**, 67357-67364.

**36** H. Iwamochi, T. Hirose, Y. Kogawa and A. Yoshizawa, *Chem. Lett.* 2010, **39**, 170-171.

**37** M. Lee, S. T. Hur, H. Higuchi, K. Song, S. W. Choi and H. Kikuchi, *J. Mater. Chem.* 2010, **20**, 5813-5816.

**38** L. Wang, W. He, X. Xiao, Q. Yang, B. Yang, P. Li and H. Yang, *J. Mater. Chem*. 2012, **22**, 2383-2386.

**39** K. W. Park, M. J. Gim, S. Kim, S. T. Hur and S. W. Choi, *ACS Appl. Mater. Interfaces* 2013, **5**, 8025-8029.

**40** M. Grunert, R. A. Howie, A. Kaeding and C. T. Imrie, *J. Mater. Chem*. 1997, **7**, 211-214.

**41** F. Ely, G. Conte, A. Merod-likeo and H. Gallardo, *Liq. Cryst*. 2004, **31**, 1413-1425.

**42** W. L. He, G. H. Pan, Z. Yang, D. Y. Zhao, G. G. Niu, W. Huang, X. T. Yuan, J. B. Guo, H. Cao and H. Yang, *Adv. Mater*. 2009, **21**, 2050-2053.

**43** A. Hauser, M. Thieme, A. Saupe, G. Heppke and D. Kruerke, *J. Mater. Chem.* 1997, **7**, 2223-2229.

**44** C. V. Yelamaggad, I. S. Shashikala, G. Liao, D. S. S. Rao, S. K. Prasad, Q. Li and A. Jakli, *Chem. Mater., 2006,* **18**, 6100-6102.

**45** A. Yoshizawa, M. Sato and J. Rokunohe, *J. Mater. Chem.*, 2005, **15** 3285-3290.

**46** M. L. Rahman, S. M. Sarkar, M. M. Yusoff, S. Kumar and C. Tschierske, *RSC Adv*., 2015, **5**, 87019-87029.

**47** M. Caricato, A. K. Sharma, C. Coluccini and D. Pasini, *Nanoscale,* 2014, **6**, 7165-7174.

**48** M. Caricato, A. Delforge, D. Bonifazi, D. Dondi, A. Mazzanti and D. Pasini, *Org. Biomol. Chem.,* 2015, **13**, 3593-3601.

**49** M. Aqnes, A. Nitti, D. A. V. Griend, D. Dondi, D. Merli and D. Pasini, *Chem. Commun.*, 2016, Advance Article, DOI: 10.1039/C6CC05937F.

**50** A. Nafees, A. Sinha, N. V. S. Rao, G. Kalita, G. Mohiuddin and M. K. Paul, *RSC Adv*., 2016, **6**, 43069-43079.

**51** N. Gimeno, L. Pintre, M. M. Abadia, J. L. Serrano and M. B. Ros, *RSC Adv*., 2014, **4**, 19694-19702.

**52** S. Dhakai and J. V. Selinger, *Phys. Rev. E*, 2011, **83**, 020702.

**53** C. C. Han, Y. C. Chou, S. Y. Chen and H. C. Lin, *RSC Adv.,* 2016, **6**, 32319-32327.

**54** K. Aihara, K. V. Le, M. Isobe, Y. Sasaki, J. Mieczkowski, H. Takezoe and K. Ema, *Ferroelectrics*, 2012, **431**, 1-5.

**55** W. Zhang, W. He, C. Di, X. Wang, Z. Yang, D. Wang, H. Cao, D. Yang and H. Yang, *Liq. Cryst.* 2016, **43**, 524-534.

**56** M. Marik, A. Mukherjee, D. Jana, A. Yoshizawa and B. K. Chaudhuri, *Phys. Rev. E*, 2013, **88**, 012502.

**57** J. Rokunohe and A. Yoshizawa, *J. Mater. Chem*., 2005, **15**, 275-279.

**58** J. Rokunohe, A. Yamaguchi and A. Yoshizawa, *Liq. Cryst.*, 2005, **32**, 207-212.

**59** A. Yoshizawa, *Mol. Cryst. Liq. Cryst.* 2014, **595**, 29-38.

**60** H. Liu, D. Shen, X. Wang, Z. Zheng and S. Li, *Opt. Mater. Express*, 2016, **6**, 436-443.

**61** S. Aya, a. Zep, K. Aihara, K. Ema, D. Pociecha, E. Gorecka, F. Araoka, K. Ishikawa and H. Takezoe, *Opt. Mater. Express*, 2014, **4**, 662-671.

**62** M. Tanaka and A. Yoshizawa, *J. Mater. Chem. C*, 2013, **1**, 315-320.

**63** Y. Zhang, Y. Guan, S. Yang, J. Xu and C. C. Han, *Adv. Mater.* 2003, **15**, 832-835.

**64** A. Rochefort, E. Bayard and S. H. Messaoud, *Adv. Mater.* 2007, **19**, 1992-1995.

**65** R. B. Balakrishna and N. Ashwini, *Cryst. Growth Des.* 2003, **3**, 547-554.

View Article Online
DOI: 10.1039/C6RA19266A ARTICLE

**66** J. A. Bis, P. Vishweshwar, D. Weyna and M. J. Zaworotko, *Mol. Pharm.* 2007, **4**, 401-416.

**67** T. R. Shattock, K. K. Arora, P. Vishweshwar and M. J. Zaworotko, *Cryst. Growth Des*. 2008, **8**, 4533-4545.

**68** J. Guo, Y. Shi, X. Han, O. Jin, J. Wei and H. Yang, *J. Mater. Chem. C*, 2013, **1**, 947-957.

**69** Y. Li, Y. Cong, H. Chu and B. Zhang, *J. Mater. Chem. C*, 2014, **2**, 1783-1790.

**70** M. J. Frisch, G. W. Trucks and H. B. Schlegel, et al., Gaussian 09, Revision A.1, Gaussian, Inc., Wallingford, CT, 2009.

**71** S. Grimme, *J. Comput. Chem*., 2006, **27**, 1787–1799.

**72** B. H. Besler, K. M. Merz Jr and P. A. Kollman, *J. Comput. Chem*., 1990, **11**, 431–439.

**73** C. L. Wei, T. C. Chen, P. Raghunath, M. C. Lin and H. C. Lin, *RSC Adv*., 2015, **5**, 4615-4622.

**74** L. Y. Wang, S. Y. Tan and H. C. Lin, *Macromolecules*, 2010, **43**, 1277-1288.

View Article Online
DOI: 10.1039/C6RA19266A

RSC Advances

RSCPublishing

ARTICLE

## Table of Contents (TOC)/Graphical Abstract

The first series of liquid crystalline supramolecular diads **C**/**D** containing asymmetric rod-like and H-bonded bent-core mesogens were designed and synthesised, among which supramolecular diad $\mathbf{P_{III}}$*/$\mathbf{A_{II}}$* with two chiral centers on both H-acceptor/H-donor and non-lateral fluoride substitution possessed a wide blue phase I (BPI) range of 13.7°C. According to the molecular modeling, a large biaxial parameter ($W_1/W_2 \geq 3.2$) and an appropriate HTP value (4.2-4.8 $\mu m^{-1}$) are the most important factors to stabilize the double twisted cylinder structure (i.e., BPI) in supramolecular diads.